CONF-810831--103

Conf-810831--103

DE83 007942

Paper presented at the *Second Topical Meeting on FUSION REACTOR MATERIALS*, August 9-12, 1981, Seattle, Washington; and for publication in the *Proceedings*.

DISCLAIMER

IMPORTANT MATERIAL CONSIDERATIONS IN INTOR*

M. A. Abdou, R. F. Mattas, and D. L. Smith
Argonne National Laboratory
Argonne, Illinois 60439

and

G. L. Kulcinski
University of Wisconsin
Madison, Wisconsin 53706

*Work supported by the U. S. Department of Energy.

IMPORTANT MATERIAL CONSIDERATIONS IN INTOR*

M. A. Abdou, R. F. Mattas, and D. L. Smith
Argonne National Laboratory
Argonne, Illinois 60439

G. L. Kulcinski
University of Wisconsin
Madison, Wisconsin 53706

A number of important material-related problems were identified and analyzed during the Phase-I study for INTOR. The first wall and divertor collector plate are subjected to severe normal and off-normal conditions. A melt layer is predicted to develop in a bare stainless steel wall under plasma disruptions. Graphite tiles will not melt but they introduce other serious uncertainties into the design. The design strategy for the divertor collector plate focused on separating the surface and high heat flux problems and on utilizing a novel mechanical design concept for attaching tungsten tiles to a stainless steel (or copper) heat sink.

1. INTRODUCTION

The International Tokamak Reactor (INTOR) Workshop is a collaborative effort among the USA, USSR, EURATOM, and Japan. The effort is conducted under the auspices of the International Atomic Energy Agency (IAEA). The purposes of the INTOR Workshop are to define the objectives of, assess the technical feasibility of, and develop a design for the appropriate next major experiment in the worldwide tokamak program.

The Zero-Phase [1] of the INTOR Workshop was conducted during 1979. The conclusion of this Zero-Phase is that the operation by the early 1990s of an ignited, deuterium-tritium burning tokamak experiment that could serve as an engineering test facility is technically feasible, provided that the supporting research and development activity is expanded immediately.

As a result of this positive conclusion, the INTOR Workshop was extended into Phase-I, the definition phase in 1980. The objective of the Phase-I Workshop is to develop a conceptual design of INTOR. Phase-I was completed in July 1981 [2-6].

The INTOR Workshop has played a major role in identifying and focusing the attention of the world fusion community upon the major problems that must be addressed before the next major experiment in the tokamak program can be undertaken. The Workshop has also made a major contribution in developing a consensus on the most likely solutions to these problems.

This paper presents a summary of key material problems that emerged from a comprehensive design study, conducted during Phase-I of the INTOR Workshop, for the first wall and divertor.

*Work supported by the U.S. Department of Energy.

2. INTOR DESIGN STUDY — OBJECTIVES AND PARAMETERS

INTOR is conceived to be the maximum reasonable step beyond the next generation of large tokamaks (TFTR, JET, JT-60, and T-15) in the world fusion program. It should provide physics and engineering data relevant to the construction of a fusion demonstration power plant. The specific technical objectives of INTOR are summarized in Table 1. Those technical objectives will be achieved at different stages of INTOR operation. The staged operation schedule proposed for INTOR is shown in Table 2.

Table 1. INTOR Technical Objectives

A. Reactor-Relevant Mode of Operation
1. Ignited D-T plasma.
2. Controlled >100-s burn pulse.
3. Reactor-level particle and heat fluxes ($P_n \geq 1$ MW/m^2).
4. Optimized plasma performance.
5. Duty cycle $\geq$70%.
6. Availability 25-50%.
B. Reactor-Relevant Technologies
1. Superconducting toroidal and poloidal coils.
2. Plasma composition control (e.g., divertor).
3. Plasma power balance control.
4. Plasma heating and fueling.
5. Blanket heat removal and tritium production.
6. Tritium fuel cycle.
7. Remote maintenance.
8. Vacuum.
9. Fusion power cycle.
C. Engineering Test Facility
1. Testing of tritium breeding and extraction.
2. Testing of advanced blanket concepts.
3. Materials testing.
4. Plasma engineering testing.
5. Electricity production, $\sim$5-10 MWe.
6. Fluence $\sim$5 MW-yr/m^2 during Stage III for component reliability and materials irradiation testing.

Table 2. Staged Operation Schedule

Stage	No. Years	Emphasis	Availability (%)	Annual 14-MeV Neutron Fluence ($MW\text{-}yr/m^2$)[a]	Annual Tritium Consumption (kg)
IA	1	Hydrogen plasma operation, engineering checkout	10	——	——
IB	2	D-T plasma operation	15	0.16	3.6
II	4	Engineering testing	25	0.31	6.9
III	8	Ungraded engineering[b] testing	50	0.62	13.8

[a]At the outboard location of the test modules.

[b]The objective is to achieve ~5 $MW\text{-}yr/m^2$ within ≤10 y after the end of Stage II. This could be achieved in several ways; the case given here is only representative.

A conceptual design has been developed for a device that can fulfull the INTOR technical objectives. The major design parameters are given in Table 3. Ignition is predicted to be achievable with some margin for plasma physics uncertainties. Neutral beams are used for plasma supplementary heating. A single-null divertor, with the chamber at the bottom, has been selected for impurity control.

Table 3. INTOR Major Design Parameters

Chamber major radius, m	5.2
Plasma minor radius, m	1.2
Plasma elongation	1.6
Plasma chamber area, m^2	380
Field on axis, T	5.5
Inner blanket/shield thickness, m	1.2
Outer blanket/shield thickness, m	1.5
Burn average beta, $\bar{\beta}_t$ %	5.6
Plasma current, MA	6.4
Average neutron wall load, MW/m^2	1.3
Peak thermal power, MW	620
No. of TF coils	12
Plasma burn time, s	
Stage I	100
Stages II, III	200
Plasma duty cycle	
Stage I	0.7
Stages II, III	0.8
No. of lifetime pulses	7×10^5
No. of beam injectors	5
Beam power, MW	75
Beam energy, keV	175

3. FIRST WALL

The design and performance of the first wall received considerable attention in the INTOR studies. Several options were proposed and key issues were addressed in considerable detail. The details of the analysis performed by the four countries during Phase-I are documented in the reports issued by EC [3], Japan [4], USA [5], and USSR [6].

The first-wall system as defined in the present study, which generally consists of the plasma chamber and serves as the first physical barrier for the plasma, consists of the following components:

- An outboard wall that serves as the major fraction of the plasma chamber surface and receives particle and radiation heat loads from the plasma and radiative heating from the divertor.
- An inboard wall that receives radiative and particle flux during the plasma burn and the major fraction of the plasma energy during a disruption.
- A limiter region on the outboard wall that serves to form the plasma edge during the early part of startup.
- A beam-shine-through region on the inboard wall that receives shine-through of the neutral beams at the beginning of neutral injection.
- A ripple armor on the outboard wall that receives enhanced particle fluxes caused by ripple effects during the late stages of neutral injection.

These regions are illustrated in the first-wall configuration shown in Figure 1.

3.1 Operating Conditions

The reference operating schedule for INTOR based on three stages of operation was shown in Table 2. The operating parameters for the INTOR first wall and its special regions are given in Table 4. As can be seen from this table, the first wall is subjected during the plasma burn to: (1) an average neutral wall load of 1.3 MW/m^2; (2) a surface heat load of 11.6 W/cm^2 from plasma radiation (10.5 W/cm^2) and particles (1.1 W/cm^2); and (3) a charge-exchange (cx) flux of 3.3×10^{20} $m^{-2}s^{-1}$ with an average energy of 200 eV. In addition to these loads that are constant during the plasma burn, special regions of the first wall receive significant heat and

Table 4. INTOR First-Wall Operating Parameters

First Wall	
Total plasma chamber area, m^2	380
Average neutron wall loading, MW/m^2	1.3
Radiative power to first wall, MW	40
Charge-exchange	
Power, MW	4
Current (50% D, 50% T), s^{-1}	1.3×10^{23}
Flux, $m^{-2}s^{-1}$	3.3×10^{20}
Energy, eV	200
Cycle time (Stage I/Stage II & III), s	145/245
Burn time (Stage I/Stage II & III), s	100/200
Total disruption energy, MJ	220
Disruption time, ms	20
Operating life, y	15 y
Total average neutron flux, n/m^2	6.8×10^{26}
Total 14-MeV neutron flux, MW-y/m	6.5
Total number shots	7.1×10^5
Total number disruptions	1080
Outboard Wall	
Area, m^2	266
Surface heat flux, W/cm^2	
From plasma	11.6
From divertor	3.4
Total	15
Average nuclear heating, W/cm^3	15
Limiter (Outboard wall at $R \sim 6$ m - Upper and Lower)	
Width, m	1
Area (each), m^2	38
Total ion flux, s^{-1}	3×10^{23}
Total heat flux, MW	10
Total ion heat flux, MW	5
Heat flux density, MW/m^2	0.3
Peaking factor	1.5
Typical particle energy, eV	100
Duration, s	4
Period, s	t = 0-4
Ripple Armor (Outboard wall at R = 6 m - Upper and Lower) (Does not coincide with the limiter.)	
Area, m^2	26
Heat flux (ripple = ±0.5%), MW/m^2	0.4
Peaking factor	2
Particle energy (D), keV	120
Period, s	t = 8-10
Inboard Wall	
Area, m^2	114 m^2
Surface heat flux, W/cm^2	11.6
Average nuclear heating, W/cm^3	10
Peak disruption energy density, J/cm^2	289
Beam-Shine-Through Region (Inboard Wall)	
Total power (5% of injected), MW	4
Particle energy, keV	175
Duration, s	2
Period, s	t = 4-6
Area, m^2	4
Heat flux, MW/m^2	1

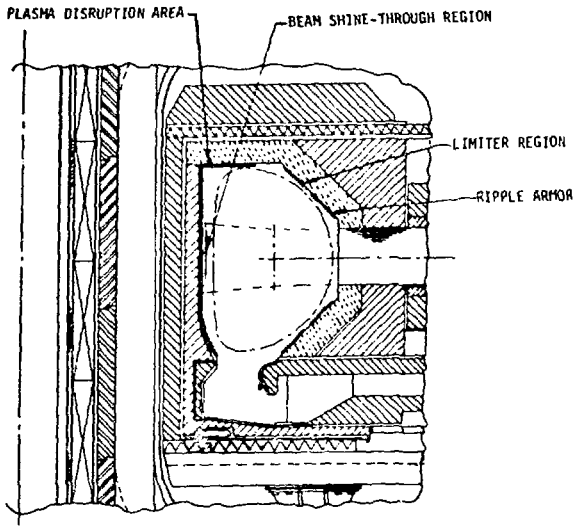

Figure 1: Schematic for first-wall configuration showing special regions that receive higher heat and particle fluxes.

particle loads during plasma startup and off-normal conditions. The "startup limiter" receives a maximum ion flux of 7.9×10^{20} $m^{-2}s^{-1}$ with an average energy of 100 eV in the period of 0-4 s from the beginning of the startup. There are two limiters, one at the upper and the other at the lower parts of the outboard wall. The particle load can be shared between the two limiters in successive time periods during the 4 s. The "beam-shine-through" region is on the inboard wall opposite the neutral beam openings located outboard. When the beam injectors are turned on the plasma density is low and a part of the beam power penetrates and gets deposited on the beam-shine-through region. The peak power at the beam-shine-through region depends strongly on the plasma startup scenario. As shown later, constraints on maximum temperature of structural material limit the allowable heat load to $\lesssim 1$ MW/m^2.

Physics analysis during the INTOR study revealed that the presence of a finite field ripple will cause a loss of some beam ions near the end of the beam injection period. These ripple ions will result in an average heat load of 0.4 MW/m^2 on a toroidal strip in the outboard region for a period of 2 s. A peaking factor of 2 is assumed.

The most serious off-normal occurence identified is a plasma disruption. There are considerable uncertainties in specifying the characteristics of plasma disruption, particularly as to the frequency of occurence, location of energy dump, disruption time constant, and the value of peak energy deposition. The disruption scenario for INTOR assumes 1080 disruptions to occur during the device lifetime. A peaking factor of 5 results in a peak energy density of 289 J/cm^2. The power density is assumed constant during a disruption time of 20 ms. The plasma energy is deposited in the inboard region as shown in Figure 1.

3.2 Design Goals

An important design goal adopted for the INTOR first wall was that it should survive the full lifetime of the device. INTOR life is 15 y, which corresponds to 6.5 $MW\text{-}y/m^2$ integral neutron wall load and 7.1×10^5 plasma cycles.

Unscheduled failures of parts of the first wall are expected to occur. The design strategy to minimize the number and impact of unscheduled failures consists of two elements. First, the design of the first wall must be kept simple enough to minimize unscheduled failures. Design complexity normally leads to increased uncertainties in characterizing the performance of the first wall and increases the potential for occurence of unexpected failures. Second, the first wall must be designed for ease of replacement to recover from unscheduled failures.

3.3 Design Options

Two options for the design of the first wall emerged as worthy of detailed considerations. The two options are: (1) full bare stainless steel wall; and (2) radiately-cooled graphite tiles in the inboard region (where disruptions occur) with bare stainless steel in the outboard region.

The major advantages of the full bare stainless steel wall are: (1) design simplicity; and (2) less uncertainties than any of the other design options investigated. The major uncertainty in this design option relate to the stability of the melt layer, which is predicted to form during a disruption (see next section). The principal advantages of the graphite tile concept are that graphite will not melt under plasma disruptions and it does not need active cooling. However, a number of serious concerns have been identified for this concept. These are:

(1) Substantial increase in the heat flux to the outboard wall. The thick ($\sim$4 cm) graphite tiles generate $\sim$40 MW of additional nuclear heat that must be radiated to the outboard wall and the wall behind the tiles.

(2) Serious potential problems with mechanical support of tiles:

- The hot graphite tile may carburize or overheat the cooled support fitting and cause its failure.
- Cooled support rail may provide excessive constraints or cooling to local portions of the tile and result in cracking due to thermal stresses.
- Shock loads applied to the tile during a plasma disruption may cause the tile support to break.

(3) Safety concerns with combustion of hot graphite in air (400 GJ of energy compared to 40 GJ in TF coils).

(4) Magnitude of chemical sputtering is uncertain.

(5) Resistance to radiation damage is uncertain.

(6) The large amount of the graphite eroded may cause significant problems in the regions where it is deposited.

Research and development programs to resolve the critical issues associated with the two design concepts identified above are urgently needed to make a justified design selection for the first wall design.

3.4 Reference Design

A full bare stainless steel wall was selected for INTOR for the purpose of developing a self-consistent reference design. All first wall components are fabricated from Type 316 stainless steel and utilize low-pressure (<1 MPa) water coolant. Figure 2 is a schematic diagram of the panel-type construction showing the thicker flat panel that faces the plasma and the corrugated back panel that forms the coolant channels. The two panels are diffusion bonded together and welded supports are spaced as required. The thickness of the plasma side panel is sufficient to withstand the sputtering and vaporization erosion predicted for the full life of the reactor. The present design philosophy was to avoid incorporating any separate armors for the special high heat flux regions, if possible, in order to keep the first wall system design as simple as possible. As a result, the special regions, viz., limiter, beam-shine through and ripple-armor region, are just a part of the first wall with minor thickness modifications to allow for effects caused by the preferential heat or particle fluxes.

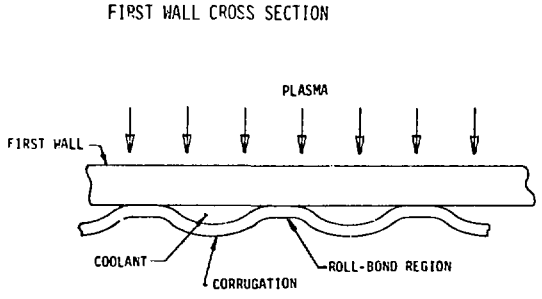

Figure 2. First-wall cross section.

The reference first-wall design is a water-cooled stainless steel panel. The low temperature water coolant maintains the structure at low temperature which provides acceptable structural properties under irradiation. The low pressure also tends to minimize primary stress requirements. The 20% cold-worked stainless steel is selected because of superior radiation damage resistance and the higher allowable design stress. The panel-type construction is proposed because of ease of fabrication, reduced stresses resulting from the thin corrugated coolant channels, and longer predicted lifetime than that for tube-bank designs. The outboard wall is an integral part of the blanket and serves as the containment for the neutron multiplier. This tends to minimize structure and coolant volumes between the plasma and the breeder zone, which enhances the breeding performance. The manifolding and support structure are readily incorporated with the blanket.

The reference stainless steel first-wall design meets all design requirements and is predicted to last the full reactor lifetime under the reference operating conditions. The design and lifetime analyses provided for (1) sputtering, blistering and vaporization erosion allowances; (2) maximum structural temprature limits; (3) maximum stress limits for the structure; and (4) fatigue limits of the structure. Table 5 summarizes the results of the lifetime analysis for the various regions of the first wall.

The thicknesses of the various regions of the first wall shown in Table 5 allow for a 3-mm end-of-life thickness. The physical sputtering erosion rates are based on effective sputtering yields of 0.017 atoms per particle at 100 eV.

3.4.1 Disruption Effects

Three effects of plasma disruptions on the first wall were analyzed in the present study, viz., vaporization of the wall, formation of a melt layer, and electromagnetic loading. A comprehensive modeling effort was undertaken and analyses performed by all participating countries to evaluate the extent of vaporization and melt layer formed during a plasma disruption. Figure 3 summarizes the calculated thickness of the vaporized region and melted region of stainless steel for various energy densities. The reference condition is 289 J/cm^2 during a 20-ms disruption. The vaporized thicknesses are considered acceptable. However, if the melted layer is eroded during the disruption, the erosion rates of stainless steel would be excessive. The surface region is molten less than 30 ms and the regions 50 μm into the wall are molten for only a few milliseconds.

Preliminary analyses of the electromagnetic forces induced in the first walls and in the melted regions were conducted. Calculated pressures in the stainless steel melt zone are less than 275 N/m^2 (0.04 psi). The maximum force on an 18-mm OD × 10-mm ID stainless steel tube is 2.35 kN/m. The magnitude of the force reaches a maximum before melting occurs. Also, the force reverses direction and becomes compressive at ∿12 ms for the reference disruption scenerio.

Table 5. Summary of Lifetime Analysis

Region	Total Thickness (mm)	Maximum Erosion (mm)	Maximum[a] Temp. (°C)	Maximum[b] Stress (MPa)	Fatigue Life, Cycles	
					No Erosion	W/Erosion[c]
Outboard wall	11.7	8.7[d]	260	360	3×10^6	$>10^7$
Ripple region	11.7	8.7[d]	297	400	1×10^6	$>10^7$
Limiter region	12.8	9.8[d]	280	410	8×10^5	$>10^7$
Inboard wall	13.5	10.5[e]	275	408	9×10^5	$>10^7$
Beam-shine-through region	13.5	10.5[e]	332	495	2×10^5	$>10^7$

[a]Maximum specified temperature = 350°C.

[b]Maximum allowable stress = 650 MPa plasma side, 765 coolant side (cold-worked material).

[c]Assumes erosion rate one-half of predicted rate for conservative design.

[d]Physical sputtering.

[e]Physical sputtering plus vaporization.

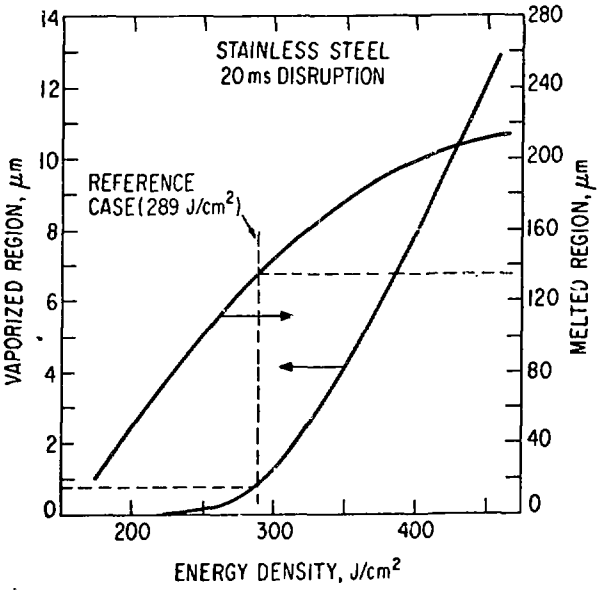

Figure 3: Calculated vaporized and melted regions as a function of energy for a 20-ms disruption.

3.4.2 Thermal Hydraulics

The thermal responses of the various regions of the first wall are summarized in Figures 4-6. for the specified wall thicknesses and heating rates. Figure 4 shows the thermal response of the 11.7-mm outboard wall and the ripple armor region for Stage IB operation (100-s burn). The wall temperatures remain approximately the same for the extended burn during Stage II and III operation. The maximum temperature of ∿260°C near the end of the burn is within the 350°C maximum temperature limit specified. This temperature would be slightly less for the case of the actively cooled limiter. The 297°C thermal spike on the surface of the ripple armor region is also within the allowable temperature limits. Figure 5 shows the thermal response for the 12.8-mm thick limiter region. The temperature near the end of the burn (280°C) is

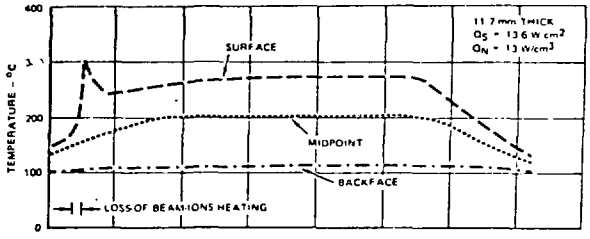

Figure 4: Thermal responses of outboard wall and ripple armor region.

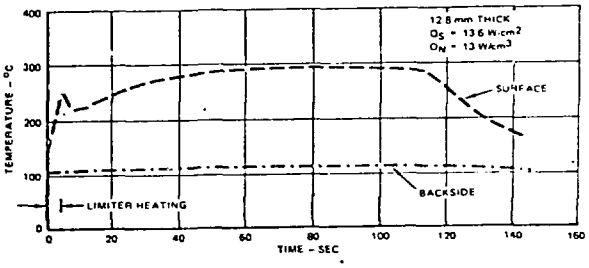

Figure 5: Thermal response of limiter region.

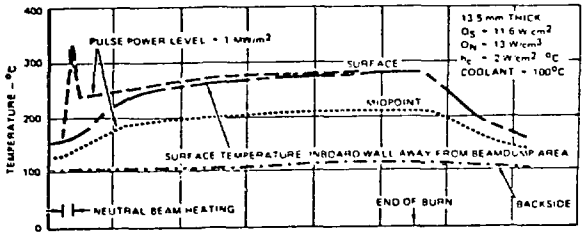

Figure 6: Thermal responses of inboard wall and neutral beam-shine-through region.

slightly higher than that of the outboard wall because of the increased wall thickness; however, the 250°C thermal spike associated with startup is considerably less than the steady-state temperature. The thermal response of the inboard wall is shown in Figure 6. The higher steady-state temperature of the inboard wall (275°C) compared to the outboard wall is due primarily to the higher bulk heating in the thicker in-

board wall. The neutral beam-shine-through produces a 332°C thermal spike during startup if the heat flux is 1 MW/m^2 for 2 s. A 3-MW/m^2 heat flux for the same period produces a thermal spike of ∿700°C on the surface. Calculations indicate no thermal spike occurs at mid-thickness of the panel.

3.4.3 Stress/Lifetime Analysis

Stress and lifetime analyses have been performed to guide the design of the INTOR first wall. Pressure loading, thermal loading and magnetic loading resulting from plasma disruption have been considered in the stress analysis. The analyses have taken into account the thinning of the first wall due to sputtering and vaporization. Stresses due to differential swelling have been assumed to be small in the present analysis. The lifetime analyses of the first wall have been performed for bare stainless steel as well as for stainless steel coated with beryllium under the reference operating parameters. In addition to a solid first wall, the performance of a grooved first wall has also been evaluated.

For the reference operating scenario, viz., 7.1 × 10^5 cycles and 1083 disruptions over a 15-y life, a solid outboard wall constructed of an 11.7-mm thick, 20% cold-worked stainless steel panel can meet the 15-y design life requirement for stress and fatigue life (see Table 5). The maximum allowable surface heat flux corresponding to a fatigue life of 7.1 × 10^5 cycles is shown in Fig. 7 as a function of wall thickness and the nuclear heating rate. The allowable heat flux (dotted lines) is greater than the expected heat flux in all cases. The cold-worked stainless steel provides a significantly larger design margin than annealed material for the maximum stress limit. Also, the design margin for fatigue life is substantially increased if advantage is taken of the reduced stresses that result from wall erosion. A conservative value of one-half of the predicted erosion rate gives a design life in excess of 10^7 cycles. Similar results are derived for the 12.8-mm thick limiter region.

If the melt layer formed during a disruption does not erode, a solid inboard wall (13.5 mm) constructed of cold-worked stainless steel will meet the full 15-y design life. In order to meet the full life requirement for the beam-shine-through region, one must take advantage of the decreasing thermal stresses that result from thinning caused by erosion. If at most 10-12% of the melt layer erodes during the disruptions, a grooved stainless steel inboard wall ∿30-mm thick will survive the full 15-y design life.

Coolant channels can be constructed out of thin-walled (3-4 mm) corrugated panels that are welded to the back of the first wall. These panels should have sufficient fatigue life provided the water chemistry is adequately controlled to prevent early failure due to stress corrosion or corrosion fatigue.

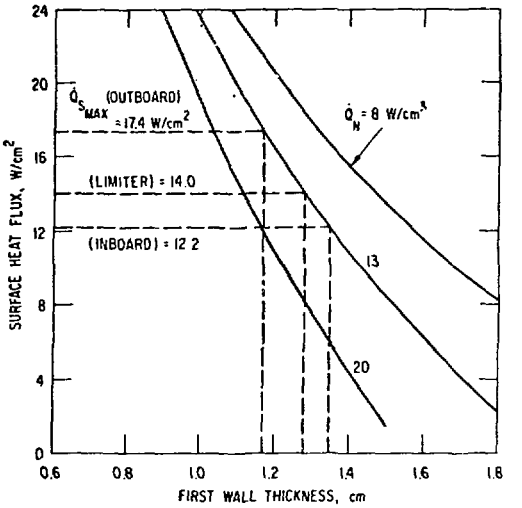

Figure 7: Allowable maximum surface heat flux in a Type 316 stainless steel wall for a fatigue life of 7.1 × 10^5 cycles, as a function of wall thickness and nuclear heating rate.

4. DIVERTOR COLLECTOR PLATE

The impurity control system in INTOR is a single null poloidal divertor located at the bottom of the plasma chamber, shown in Figure 1. The purpose of the divertor is to collect the ionized particles that have escaped from the plasma along with the sputtered particles from the first wall. The divertor effort for INTOR considered the important aspects of physics, magnetics, engineering, and maintenance. A summary of the operating conditions is shown in Table 6. The total power to the divertor is 80 MW, which is equally divided between the inner and outer channels. A total of 70 MW of that power impinges directly on the divertor collector plates resulting in high surface heat and particle fluxes, in addition to the usual neutron flux. The inner plate is placed out an angle of 30 deg and the outer plate is placed at an angle of 14.5 deg with respect to the separatrix. The angular placement reduces the peak surface heat flux to 2 MW/m^2 and the peak particle flux to 1.5 × 10^{22}/m^2-s.

The severe operating conditions make the divertor collector plate the most heavily damaged torus component. The key design issues for the collector plate are:

- Sputtering loss of material.
- Thermal stress and fatigue.
- Radiation damage, e.g. swelling and embrittlement.
- Redeposition of eroded material from the first wall and collector plate.

Table 6. Divertor Operating Conditions

Total power to divertor, MW	80
Ion power to divertor plates, MW	35
Electron power to divertor plates, MW	35
Ion flux to divertor plates, s^{-1}	5.5×10^{23}
Average energy of ions, eV	400
Composition of ions, %	
T	47
D	47
He	5
C	0.5
O	0.5
Neutral gas density at front of divertor plates, m^{-3}	10^{19}
Peak power flux to divertor plates normal to separatrix, MW/m^2	
Outboard	8
Inboard	4
Peak ion flux to divertor plates perpendicular to separatrix, M^2-s^{-1}	
Outboard	6×10^{22}
Inboard	3×10^{22}
Inclination of divertor plate to separatrix, deg	
Outboard	14.5
Inboard	30
Total power to throat and channel, MW	10
Charge-exchange neutrals, MW	5
Radiation, MW	5
Total neutral flux, s^{-1}	1.6×10^{23}
Average energy of neutrals, eV	200
Peaking factor of flux	2
Area on which the neutrals impinge,[a] m^2	33

[a] 5 strips of length 0.2 m each, 4 of them being adjacent to the ends of the divertor plates and the fifth on the wall facing the outside divertor plate.

— Electromagnetic forces induced in the collector plate during plasma disruptions.

— Tritium permeation into the collector plate coolant.

— Maintainability of the collector plate which requires periodic replacement.

During Phase I, several potential design concepts for a divertor collector plate were analyzed, and two designs were then selected and analyzed in further detail. In both designs, the problems of sputtering are separated from the problems of cooling and structural support. The designs employ a low sputtering protection plate that is attached to a heat sink composed of a standard structural alloy. The main difference between the designs is in the method of attachment of the protection plate to the heat sink. One design employs a braze to produce a high thermal conductance path and a strong bond to the heat sink (high conductance design). The other design employs mechanical attachments that produce a low thermal conductance path and a weak bond to the heat sink (low conductance design). The two designs are compared in Figure 8.

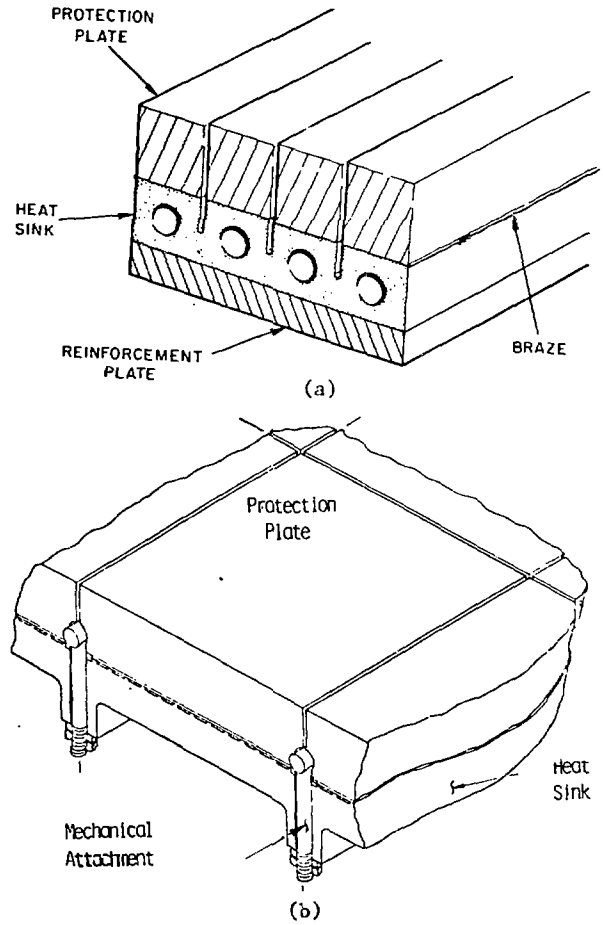

Figure 8: Divertor collector plate designs: (a) high conductance; and (b) low conductance.

The two designs result in considerably different operating conditions, as shown in Table 7. The high conductance concept has plate operating temperatures of 400-500°C compared with 2000-2300°C for the low conductance concept. At the high operating temperatures of the low conductance design, 40-50% of the incident heat is radiated back to the divertor chamber and the plasma chamber. The thermal radiation loss reduces the thermal gradient in the protection plate and the heat flux to the heat sink compared to the high conductance design. The high

strength of the braze joint in the high conductance design results in high stresses at the bond interface due to the different rates of thermal expansion of the protection plate and heat sink. The high stresses may produce fatigue crack growth and failure. The attachments in the low conductance design allow the protection plate to freely expand and rotate during the burn cycle, inducing very low stresses through the plate.

The primary materials issue for both designs is the high sputtering rate that will result in large material losses. Based upon available physical sputtering data and models, the high-Z elements are predicted to have the lowest sputtering rates for an incoming particle energy of ~400 eV. The sputtering analysis for INTOR has focused on the high-Z refractory metals such as molybdenum, tungsten, and their alloys. The physical sputtering rates of two materials, tungsten and ZM-6 (a molybdenum alloy), were analyzed during Phase-I, and the predicted sputtering behavior is shown in Table 8. The self-sputtering has been taken into account using the approximation

$$\eta_{eff} = \eta_{gas} \times \frac{1}{1 - 0.5\,\eta_{self}},$$

where η_{eff} is the effective sputtering coefficient, and η_{self} is the self-sputtering coefficient [2]. The effective sputtering coefficients are estimated to be 2.2×10^{-3} and 2.4×10^{-3} for tungsten and ZM-6, respectively. The resulting material loss rates are 5.22×10^{-10} m/s and 5.62×10^{-10} m/s, respectively. The estimated sputtering lifetime is 1.5-2 y at a 50% duty factor.

There are several uncertainties in the predicted value of sputtering. First, the values for tritium sputtering are extrapolations and not measured values. It is estimated that the extrapolated values can vary within a factor of 2. The values for ZM-6 have been determined by extrapolation [6] of measurements made at 10 keV, and the extrapolation may contain uncertainties up to a function of 3 in the direction of higher values. The experimental sputtering rates for pure molybdenum are much higher than those estimated for ZM-6.

The other materials issues for the high conductance design are shown in Table 7. Radiation embrittlement is expected to occur in the protection plate and heat sink materials. The ductile-brittle transition temperature of both molybdenum and tungsten have been observed to

Table 7. Comparison of High Conductance and Low Conductance Design Concepts

	High Conductance	Low Conductance
Protection plate materials	W, ZM-6	W
Heat sink materials	Cu, Zircaloy	Austenitic stainless steel
Protection plate attachment	Braze	Mechanical
Typical plate temperatures	500°C	2200°C
Heat flux to heat sink	2.4 MW/m^2	1.1 MW/m^2
Mode of cooling	Thermal conduction	Radiation-thermal conduction
Primary concerns	Physical sputtering Braze integrity Thermal fatigue Radiation embrittlement	Physical sputtering Chemical sputtering Emissivity of sputtered W Embrittlement of recrystalized W

Table 8. Sputtering Coefficients for W and ZM-6 at 400 eV

Ion	Comp. (%)	W		ZM-6	
		η	$\eta \times c$	η	$\eta \times c$
D	47	4×10^{-4}	2.88×10^{-4}	2.4×10^{-4}	0.113×10^{-3}
T	47	2×10^{-3}	0.99×10^{-3}	1.6×10^{-3}	0.75×10^{-3}
He	5	7×10^{-3}	0.35×10^{-3}	8×10^{-3}	0.4×10^{-3}
C	0.5	1×10^{-2}	0.05×10^{-3}	3×10^{-2}	0.15×10^{-3}
O	0.5	2×10^{-2}	0.1×10^{-3}	5×10^{-2}	0.25×10^{-3}
Self		0.5		0.5	
Effective			2.2×10^{-3}		2.4×10^{-3}

increase to 200-300°C after low temperature irradiation [7]. Therefore, the protection plate material must be treated as a brittle material for this design. Limited data indicate that radiation embrittlement could be severe in cold-worked copper [4]. However, since irradiation data does not exist for copper or copper alloys at high neutron fluence, there is a considerable uncertainty in the expected embrittlement for the operating conditions in INTOR. There is also a large uncertainty in the expected behavior of the braze bond. It is therefore not possible to evaluate the thermal fatigue lifetime, and additional experimental data are required for a complete evaluation.

The additional materials issues for the low conductance design are related to the high operating temperatures. Chemical sputtering of tungsten, due to the presence of 0.5% oxygen in the plasma particle flux, may be significant. If every incoming oxygen ion is able to participate in the formation of WO_3, the chemical sputtering rate is predicted to be approximately three-fourths of the physical sputtering rate. Chemical sputtering of tungsten is not well understood, however, and additional work is required. The surface temperature of tungsten depends upon the value of the emissivity. In order to achieve reasonable operating temperatures, the emissivity value should be greater than ~0.4, which requires a roughened surface. Sputtering is expected to influence the surface roughness, but the effect of sputtering on emissivity is not well characterized. If the emissivity values of a sputtered surface are low, then the operating temperatures will be excessive. It is possible to use austenitic stainless steel as the heat sink material, because of the reduced heat flux to the heat sink in this design. The stainless steel heat sink is expected to last the reactor lifetime. The materials considerations for the low conductance design are discussed in greater detail in another paper in this conference [8].

REFERENCES

[1] INTOR - International Tokamak Reactor Zero Phase: Report of the International Tokamak Reactor Workshop, Vienna, 5-16 February, 11 June-6 July, 1-23, October, and 10-19 December 1979 (IAEA, Vienna, 1980).

[2] INTOR - International Tokamak Reactor Phase One Conceptual Design (IAEA, Vienna, 1981), to be issued.

[3] European Community Contribution to the International Tokamak Reactor Phase-I Workshop (1981).

[4] Japan Contribution to the International Tokamak Reactor Phase-I Workshop (1981).

[5] U.S. Contribution to the International Tokamak Reactor Phase-I Workshop (1981).

[6] U.S.S.R. Contribution to the International Tokamak Reactor Phase-I Workshop (1981).

[7] Steichen, J. M., J. Nucl. Mater. 60 (1976) 13.

[8] Mattas, R. F. et al., Materials selection for the U.S. INTOR divertor collector plate, this conference.